The data points were next normalized for time variance by linear interpolation, and the calibration curve resulting from this data processing procedure is plotted as the dashed overlay curve of Fig. 3.

A second digital computer program was written to reconstruct side force during the oscillatory portions of the flow program. The normalized calibration curve of Fig. 3 was programed for digital simulation; at any time point, then, the total pressure integral and reaction force variables were first defined. After normalizing the force integral to a consistent 500-psi chamber pressure and time adjusting, the computer determined the value of total side force diminished by the reaction force from Fig. 3. The final side force was obtained by summing the reaction force component to the previous calculation results. This routine was repeated at each of the remaining time points.

Although the final internal aerodynamic frequency response shows a rapid amplitude attenuation at the higher frequencies, the LITVC system internal aerodynamic bandwidth is flat to 20 cps (see Fig. 4). Both phase and amplitude ratio parameters are characteristic of a first-order system with a 20-cps break frequency.

Conclusions

Based upon results of this study, the following conclusions can be stated: 1) the pressure integral method of obtaining dynamic side-force response data appears attractive from an experimental viewpoint; manual data reduction could be greatly minimized, however, by recording all data on magnetic tape, with playback; 2) the Data Sensor differential pressure transducer is suited for the present application, although acceleration sensitivity could present problems for nozzle resonant frequencies in the neighborhood of 460 cps; 3) difficulties associated with pressure transducer temperature sensitivity and the resulting zero shift phenomena can be obviated by providing sufficient calibration null and plateau regions during the motor firing duration; and 4) the application of a consistent low-pass data acquisition system in all channels of information is desirable from a noise-rejection standpoint.

Conical Rocket Nozzle Performance under Flow-Separated Conditions

SHERWIN KALT* AND DAVID L. BADAL†
Lockheed Missiles and Space Company, Sunnyvale, Calif.

Nomenclature

A = cross-sectional area of the nozzle at a particular location, in.^{2}
c_f = nozzle thrust coefficient, with pressure on outside of motor assumed to be zero
F = thrust, lb
M = Mach number (in freestream)
M^* = characteristic M in boundary layer
p = static pressure at nozzle wall, psia
U = component of fluid velocity at edge of boundary layer parallel to wall, fps
u = component of fluid velocity in boundary layer parallel to wall, fps
u^* = characteristic velocity in boundary layer $\equiv 0.6\ U$
δ = boundary-layer thickness, in.
ϵ = nozzle-expansion ratio to a particular location
γ = specific-heat ratio of fluid
α = nozzle half-angle, deg

Subscripts

a = ambient conditions
c = combustion chamber, or reservoir conditions
e = nozzle-exit plane conditions; p_e applies in absence of separation
i = conditions at initiation of shock-turbulent boundary-layer interaction
s = conditions at separation of flow
t = conditions at nozzle throat
sl = sea-level conditions
0.95 = conditions at position in nozzle where static pressure equals 0.95 ambient pressure

Received June 12, 1964; revision received November 17, 1964. The work reported here was done under U. S. Navy Contract NOW-63-0050c.

* Research Specialist, Propulsion.
† Flight Test Analysis Engineer.

Introduction

ROCKET motors designed for high-altitude use are frequently tested under off-design conditions, for example at sea level, where it is expected that the flow in the rocket nozzle will show separation for a substantial portion of the test. For a design-performance extrapolation, using the ballistic data obtained from these tests, a means must be available to describe mathematically the flow separation conditions encountered. This note defines the necessary correlations for conical nozzles based on published data and on data from a series of flow separation tests using small 5KS-4500 motors (supplied by Aerojet-General Corporation) loaded with approximately 100 lb of aluminized solid propellant. The results, presented as part of Fig. 1, are consistent with the results of others[8–15] for such fluids as liquid propellant, air, and nitrogen in nozzles with various half-angles and expansion ratios at various ambient pressures.

Arens and Spiegler[1] present an equation adapted from one first suggested by Gadd[3] which shows the pressure ratio that would result if the fluid at velocity u_i^* in a constant stagnation temperature boundary layer were brought to rest isentropically, where $u_i^* = 0.6\ U_i$. The corresponding pressure rise $p_i - p_a$ is assumed to be equal to the resultant static pressure rise at the wall. On a semiempirical basis, Gadd chose a ratio $u_i^*/U_i = 0.6$ to calculate $p_i - p_s$, the pressure rise, from the point of the initiation of the shock-turbulent boundary layer to the separation point. In the case of a nozzle, the stagnation velocity will be most closely approached at ambient pressure, not at separation pressure, and therefore the derivation can be used to calculate $p_i - p_a$ for a nozzle. Arens and Spiegler[1] extend this concept to the supersonic case where the fluid in the boundary layer initially at velocity u_i^* is subjected to normal shock before being brought to rest isentropically. Equation (5) of Ref. 1 is plotted in Fig. 1, and good correlation to the experimental data is shown.

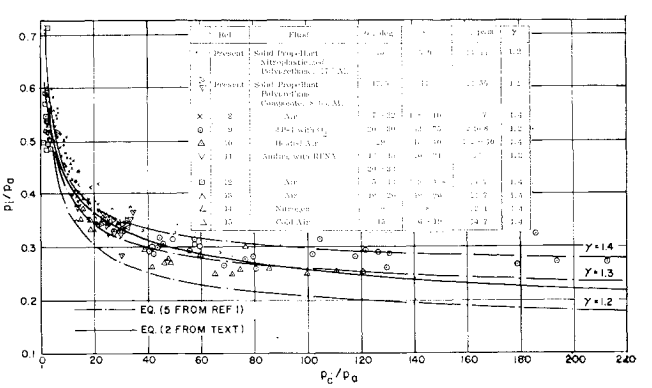

Fig. 1 Separation pressure ratio vs nozzle pressure ratio.

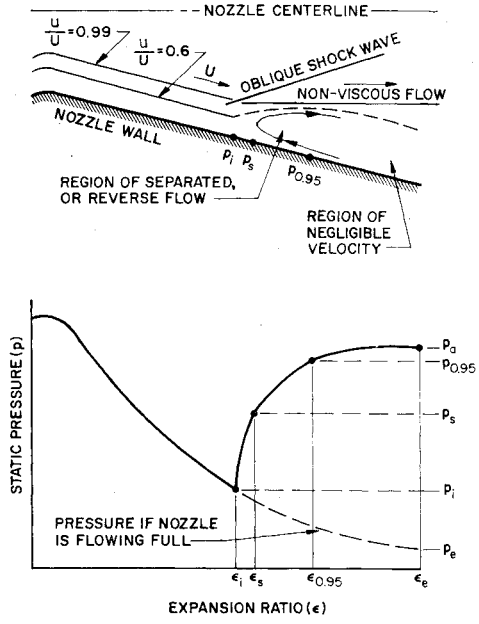

Fig. 2 Physical model of turbulent boundary layer.

Physical Model for Flow Separation in Nozzles

It is assumed that the nozzle boundary layer is turbulent in the region with which we are concerned (the data tend to substantiate this). If we accept the conclusion[2] that the pressure rise in supersonic turbulent flow is primarily determined by the shock boundary-layer interaction rather than by system geometry (step, compression corner, or an externally induced shock), then the data obtained by the investigators for configurations other than nozzles[3–6] can be used to present a physical model of nozzle-flow separation that is consistent with the equations of Ref. 1.

In Fig. 2 we diagram the different regimes postulated to exist when flow separation occurs in a nozzle. The initial point of boundary-layer thickening occurs at pressure p_i, upstream of the point of flow separation. The pressure p_i has generally been referred to as the separation pressure in empirical studies of flow separation in rocket nozzles.

The assumption[1, 2] that fluid at a characteristic velocity ratio of 0.6, in adjusting to the ambient pressure, decelerates to a negligible velocity is represented in Fig. 2 by a region of negligible velocity containing the average mass flow that existed in the boundary layer at values of $u_i \leq 0.6$. In the nozzle mainstream, adjustment to p_a occurs through an oblique shock, resulting in a region of high velocity shown as the nonviscous core. Given the mainstream flow characteristics upstream of the shock, and knowing p_i/p_a, the shock angle and downstream characteristics in the nonviscous core may be calculated. Using the model in Fig. 2, one can calculate the distance along the nozzle wall from point ϵ_i to point $\epsilon_{0.95}$. Data[2,4–6] indicate that the length of the shock boundary-layer interaction region is about 10 δ for turbulent flow, compared to approximately 100 δ for laminar flow. To calculate δ in the supersonic nozzle, a method developed by Tucker[7] was employed using the arithmetic mean temperature in the boundary layer for the computations. The results are presented in Fig. 3, where $\epsilon_{0.95} - \epsilon_i$ is the expansion-ratio difference required to accommodate the interaction region. Experimental points from many sources fall consistently closer to the shock-turbulent boundary-layer curve (10 δ) rather than the shock-laminar boundary-layer curve (100 δ). An empirical equation that gives a reasonably good approximation to these data is

$$\epsilon_{0.95} - \epsilon_i = (\epsilon_i - 1)/2.4 \tag{1}$$

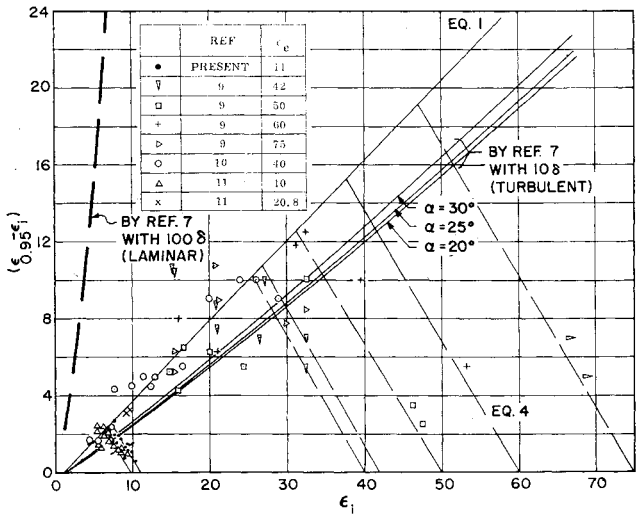

Fig. 3 Shock boundary-layer interaction region vs ϵ_i.

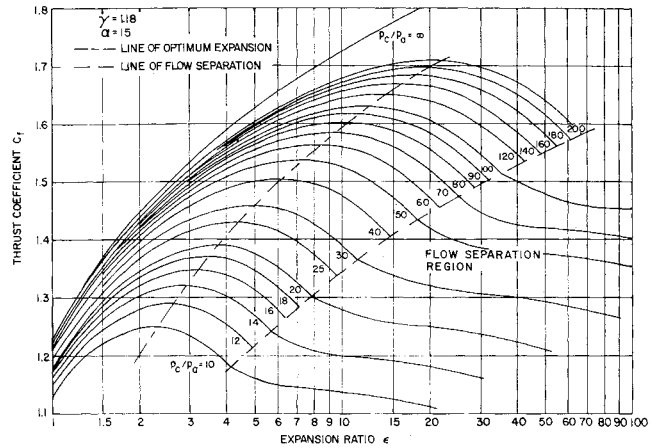

Fig. 4 Thrust coefficient vs expansion ratio.

Calculation of Sea-Level Thrust

As a first step in calculating sea-level thrust, it is necessary to determine whether the nozzle is flow-separated. The empirical equation

$$p_i/p_a = \tfrac{2}{3}(p_c/p_a)^{-0.2} \tag{2}$$

was fitted to the data as shown in Fig. 1. When p_i/p_a [from Eq. (2)] is greater than p_e/p_a, separation will occur, and the region of the interaction will begin at $p = p_i$. Thrust at sea-level conditions (flow-separated) is

$$F_{sl} = p_c A_t C_{f_i} + \int_{A_i}^{A_{0.95}} p\,dA + \int_{A_{0.95}}^{A_e} p\,dA - p_a A_e \tag{3}$$

To obtain a simple means of evaluating

$$\int_{A_i}^{A_{0.95}} p\,dA$$

the test data available were plotted in the form

$$\int_{A_i}^{A_{0.95}} \frac{p\,dA}{(p_i + p_{0.95})(A_{0.95} - A_i)}$$

the results indicating that the integral

$$\int_{A_i}^{A_{0.95}} p\,dA$$

can be set equal to 0.55 $(p_i + p_{0.95})$ $(A_{0.95} - A_i)$. (If pressure had varied linearly with area, the coefficient would have been 0.50.) Equation (1) is used to locate $A_{0.95}$. However, as the interaction region approaches the nozzle-exit plane with finite A_e, the value $(\epsilon_{0.95} - \epsilon_i)$ cannot exceed $(\epsilon_e - \epsilon_i)$ and must therefore tend to zero. This condition will be referred to as case B. In effect, as $\epsilon_i \to \epsilon_e$, the assumption that the length of the interaction region equals 10 δ is no longer valid. Some data showing this phenomenon have been plotted in Fig. 3 with the family of linear equations which has been fitted to the data

$$\epsilon_{0.95} - \epsilon_i = (\epsilon_e - \epsilon_i)/1.45 \quad (4)$$

which gives $\epsilon_{0.95} - \epsilon_i = 0$ when $\epsilon_i = \epsilon_e$, where $\epsilon_{0.95}$ corresponds to $p = 0.95\ p_a$. Solving Eqs. (1) and (4) simultaneously, we obtain the following regions of validity for cases A and B, as indicated by the upper and lower inequality signs, respectively:

$$\epsilon_i \begin{matrix} \overset{A}{\leq} \\ \underset{B}{>} \end{matrix} \frac{\epsilon_e}{1.6} + 0.38 \quad (5)$$

The region represented by

$$\int_{A_{0.95}}^{A_e} p dA$$

shows almost a constant pressure, and this term can therefore be approximated by the arithmetic average value for the region $0.975\ p_a(A_e - A_{0.95})$. Combining this with Eq. (3), we obtain the expression

$$F_{s1} = p_e A_t c_{f_i} + 0.55(p_i + p_{0.95})(A_{0.95} - A_i) - p_a(0.975 A_{0.95} + 0.025\ A_e) \quad (6)$$

The equations in this section can be used to plot nozzle performance, including flow separation, as shown in Fig. 4.

References

[1] Arens, M. and Spiegler, E., "Shock-induced boundary layer separation in overexpanded conical exhaust nozzles," AIAA J. **1**, 578–581 (1963).

[2] Chapman, D. R., Kuehn, D. M., and Larson, H. K., "Investigation of separated flows in supersonic and subsonic streams with emphasis on the effect of transition," NACA Rept. 1356, 37 (1958).

[3] Gadd, G. E., "Interactions between wholly laminar or wholly turbulent boundary layers and shock waves strong enough to cause separation," J. Aeronaut. Sci. **20**, 729–739 (1953).

[4] Bogdonoff, S. M. and Kepler, C. E., "Separation of a supersonic turbulent boundary layer," J. Aeronaut. Sci. **22**, 414–424 (1955).

[5] Liepmann, H. W., Roshko, A., and Dhawan, S., "On reflection of shock waves from boundary layers," NACA Rept. 1100 (1952).

[6] Gadd, G. E., Holder, D. W., and Regan, J. D., "An experimental investigation of the interaction between shock waves and boundary layers," Proc. Roy. Soc. (London) **A 226**, 227–253 (1954).

[7] Tucker, M., "Approximate calculation of turbulent boundary-layer development in compressible flow," NACA TN 2337 (1951).

[8] Arens, M. and Spiegler, E., "Separated flow in overexpanded nozzles at low pressure ratios," Bull. Res. Council Israel **C11**, 45 (1962).

[9] Bloomer, H. E., Antl, R. J., and Renas, P. E., "Experimental study of effects of geometric variables on performance of conical rocket exhaust nozzles," NASA TN D-846 (1961).

[10] Campbell, C. E. and Farley, J. M., "Performance of several conical convergent-divergent rocket-type exhaust nozzles," NASA TN D-467 (1960).

[11] Foster, C. R. and Cowles, F. B., "Experimental studies of gas flow separation and overexpanded exhaust nozzles for rocket motors," Jet Propulsion Lab., California Institute of Technology, Progr. Rept. 4-103 (1949).

[12] Ashwood, P. F. and Crosse, G. W., "The influence of pressure ratio and divergence angle on the shock position in two-dimensional, overexpanded, convergent-divergent nozzles," Ministry of Supply, Aeronautical Research Council, Current Paper 327 (1957).

[13] Fraser, R. P., Eisenklam, P., and Wilkie, D., "Investigation of supersonic flow separation in nozzles," J. Mech. Eng. Sci. **1**, 267 (1959).

[14] McKenney, J. D., "An investigation of flow separation in an overexpanded supersonic nozzle," Ph.D. Thesis, California Institute of Technology (1949).

[15] Ahlberg, J. H., Hamilton, S., Migdal, D., and Nilson, E. N., "Truncated perfect nozzles in optimum nozzle design," ARS J. **31**, 614 (1961).

A Kinetic Treatment of Ablation

RICHARD L. NEWMAN*

Douglas Aircraft Company, Inc., Santa Monica, Calif.

Nomenclature

b = volume density of bonds
H = enthalpy
K = Boltzmann constant
m = kinetic order of the reaction
n = number of bonds in each species
$\dot{q}$ = net heat flux to the surface
t = time
T = temperature
v = recession velocity
x = distance coordinate (fixed in space)
Z = frequency factor
α = thermal diffusivity
ϵ = activation energy
Λ = number of laminae
ν = stoichiometric factor
ξ = distance coordinate (fixed with respect to the surface)
ϕ = fraction of bonds unbroken

Subscripts

A = ablation
i = ith species
n = index
R = reaction process
s = surface
0 = interior

THE present widespread use of ablation shielding for thermal protection shows a need for a basic understanding of the mechanism of ablation. Previous analytical models have either neglected chemical reactions within a decomposing material, or have had too large a scope to permit study of internal processes. This paper reports results for the quasi-steady state for relatively uncomplicated materials. Later work will extend these results, both to cover charring materials and to eliminate some of the simplifying assumptions.

Analysis

The principal mechanism of thermal degradation of a thermoplastic, noncharring polymer is the breaking of bonds in the chain. The order and extent of bond rupture will

Received July 13, 1964; revision received August 11, 1964. Prepared under the sponsorship of the Douglas Aircraft Co. Independent Research and Development Program. The author wishes to thank W. S. Rigdon for many helpful discussions, and L. E. Weems for help in preparing the manuscript.

* Research Laboratory Analyst, Astrodynamics Branch, Advance Space Technology, Missile and Space Systems Division; on leave of absence at Department of Fuel Technology, Pennsylvania State University, University Park, Pa.